Humanes-Fuente Víctor (Orcid ID: 0000-0003-3265-5987)
Ferrero María, Eugenia (Orcid ID: 0000-0001-6858-2164)
Requena-Rojas Edilson, Jimmy (Orcid ID: 0000-0002-0653-587X)
Barichivich Jonathan (Orcid ID: 0000-0002-8223-2491)
Layme-Huaman Eva, Trinidad (Orcid ID: 0000-0003-0357-3587)

Two centuries of hydroclimatic variability reconstructed from tree-ring records over the Amazonian Andes of Peru

V. Humanes-Fuente[1], M. E. Ferrero[2], A. A. Muñoz[1,3], Á. González-Reyes[4], E. J. Requena-Rojas[5], J. Barichivich[6,7], J. G. Inga[5], and E. T. Layme-Huaman[8]

[1]Laboratorio de Dendrocronología y Estudios Ambientales, Instituto de Geografía, Pontificia Universidad Católica de Valparaíso. Valparaíso, Chile.

[2]Instituto Argentino de Nivología, Glaciología y Ciencias Ambientales, CONICET. Mendoza, Argentina.

[3]Centro de Ciencia del Clima y la Resiliencia (CR)[2]. Chile.

[4]Hémera Centro de Observación de la Tierra, Escuela de Ingeniería Forestal, Facultad de Ciencias, Universidad Mayor. Santiago, Chile.

[5]Laboratorio de Dendrocronología, Universidad Continental. Huancayo, Perú.

[6]Instituto de Conservación, Biodiversidad y Territorio, Universidad Austral de Chile. Valdivia, Chile.

[7]Laboratoire des Sciences du Climat et de l'Environnement, IPSL, CNRS/CEA/UVSQ. Gif sur Yvette, France.

[8]Instituto Nacional de Innovación Agraria. Lima, Perú.

Corresponding author: María Eugenia Ferrero (mferrero@mendoza-conicet.gob.ar)

Key Points:

- Tree rings from the Andean headwaters of the Peruvian Amazon basin allow the reconstruction of regional rainfall variability since 1817
- Reconstructed rainfall reveals imprints of El Niño and the Atlantic Multidecadal Oscillation
- There is a recurrent alternation between wet and dry periods in the past two centuries, but an increase in droughts is evident from 1980 to present

This article has been accepted for publication and undergone full peer review but has not been through the copyediting, typesetting, pagination and proofreading process which may lead to differences between this version and the Version of Record. Please cite this article as doi: 10.1029/2020JD032565

Abstract

Almost half of the tributaries of the Amazon River originate in the tropical Andes and support large populations in mountain regions and downstream areas. However, it is difficult to assess hydroclimatic conditions or to evaluate future scenarios due to the scarcity of long, high-quality instrumental records. Data from the Global Precipitation Climatology Project (GPCP) provides a complete record since 1979 and offers a good representation of rainfall over the tropical Andes. Longer records are needed to improve our understanding of rainfall variability and summer monsoon behavior at various scales. We developed the first annually-resolved precipitation reconstruction for the tropical Andes in Peru, based on tree-ring chronologies of *Cedrela* and *Juglans* species. The annual (November-October) reconstruction extends the short instrumental records back to 1817, explaining 68% of the total variance of precipitation over the 1979-2007 calibration period. The reconstruction reveals the well-documented influence of ENSO on Amazon rainfall at interannual scales (~19% of total variance), and significant multidecadal variability with alternating periods of about 40 years (~13% of rainfall variability) related to the Atlantic Multidecadal Oscillation (AMO). Both oscillatory modes can explain dry and humid periods observed within the reconstruction and are likely associated with the negative trends of rainfall in the short instrumental records and the increased drought recurrence in recent decades. Our results show that montane tropical tree rings can be used to reconstruct precipitation with exceptionally high fidelity, characterize the interannual to multidecadal variability and identify remote forcings in the hydroclimate over the Andean Amazon basin of Peru.

1 Introduction

The Amazon basin plays an important role in the South American summer monsoon (SAMS) dynamics. The large area of tropical forests modulates its own hydrological regime through the maintenance of deep atmospheric convection and recirculation of precipitation (Vera et al., 2006; Gloor et al., 2013). Over the western area of the basin, the Andes Mountains form a topographic barrier that produces a strong gradient in precipitation (Garreaud et al., 2009). The rainiest areas or "rainfall hotspot" in the Amazon basin are found in the eastern flank of the tropical Andes (Espinoza et al., 2015). Seven of the fifteen tributary rivers of the Amazon (the so called "white-water rivers") emerge from these mountain regions (Barthem et al., 2005). However, the complex topography and low density of instrumental data hinders the proper characterization of the hydroclimate variability across the region.

Analyses of the Amazon River discharge at Óbidos (77% of total drainage) indicate that the hydrological cycle of the Amazon has been intensifying during the 1990-2010 period, with an increase in the annual amplitude and severity of extreme events in the river discharge compared to previous decades (Gloor et al., 2013; Barichivich et al., 2018). Precipitation data over the Amazon basin show an upward trend in the last decades (Gloor et al., 2015) but at the same time, some extreme droughts have occurred during the years 1998 (Marengo, 2004), 2005 and 2010 (Mahli et al., 2008; Marengo et al., 2008, 2011). These results suggest an increase in climate variability, with increased moisture as a response to global climate change (e.g. Gloor et al., 2013), but with opposite drying trends affecting different sectors of the Amazon basin during the 21st century (Marengo et al., 2011; Fu et al., 2013). At regional scales, climate data from instrumental stations display complex spatio-temporal precipitation patterns. For example, rain-gauge stations over the equatorial Andes display different rainfall patterns than those in the southern tropical Andes (Segura et al., 2019). These discrepancies are in part attributed to the local variability due to the complex topography and steep climatic gradients, but also result from a scarce instrumental network and a short temporal span of satellite-based climate records. These limitations have resulted in different predictions and evaluations of precipitation trends, and a major challenge for climate modelling (particularly of precipitation) over the tropical Andes (Urrutia & Vuille, 2009).

During the monsoon season, two precipitation bands are prominent over South America: one extends from the equatorial oceans (Zhou & Lau, 1998) whilst the second belt of moisture flux convergence and convection extends from the Amazon basin towards southeastern Brazil and the adjacent ocean (the South American Convergence Zone, SACZ; Carvalho et al., 2004). Easterly winds from the tropical Atlantic Ocean and the central Amazon basin are mechanically forced by the Andes in a low-level jet structure (the South American Low Level Jet, SALLJ; Campetella and Vera, 2002; Marengo et al., 2002) and reinforces the moisture transport from the monsoon core region to tropical and subtropical latitudes (Vera et al., 2006; Garreaud et al., 2009). Precipitation variability at the monsoon region fluctuates on interannual to multi-decadal scales, largely modulated by sea-surface temperatures (SST) (Vera et al., 2006). El Niño-Southern Oscillation (ENSO) event is the major source of interannual climatic variability (Vuille & Keimig, 2004), and decadal variability has been associated for example, with the Pacific Decadal Oscillation (PDO; Garreaud et al., 2009). However, important linkages have been found between low frequency tropical rainfall variations and SST fluctuations over the tropical/equatorial Atlantic Ocean trough the Atlantic Multidecadal Oscillation (AMO; e.g. Jones and Carvalho, 2018).

To characterize the monsoon variability at long-term scales, several paleohydrological reconstructions based on speleothem and lake sediment records were generated along Brazil (Novello et al., 2012, 2016, 2018; Vuille et al., 2012; Wang et al., 2017; Wortham et al 2017), Peruvian Andes (Bird et al., 2011; Reuter et al., 2009; Apaéstegui et al., 2014; Bustamante et al., 2016; Parsons et al., 2018) and Bolivian Andes (Apaéstegui et al., 2018). Yet, knowledge on the changes in the tropical hydrological cycle between the Andes and Amazon lowlands, at high temporal resolution, is still rudimentary. To improve our understanding on the tropical Andes' hydroclimate and the interactions with the Amazon, high-resolution palaeoclimatic records are needed to bridge the gap between the (monthly-seasonal) instrumental records and long-term (often millennial) climatic proxies. Recent studies (e.g. Schöngart et al., 2002; Pereyra-Espinoza et al, 2014; Ferrero et al., 2015; Pucha-Cofrep et al., 2015; López et al., 2017; Layme-Huaman et al., 2018; Granato-Souza et al., 2018) demonstrate the feasibility of using tree-ring records to reconstruct and characterize inter-annual variability and trends in local and regional climate of the tropics in South America. Here we present the first annually resolved tree-ring rainfall reconstruction over the last two centuries from tropical Peruvian montane forests to: 1) document present and past changes in precipitation variability over the Andean headwaters of the Amazon basin, and 2) assess its relationship with large scale spatial and temporal climate forcings.

2 Materials and Methods

2.1 Study area and climatic data

The study area is located in the humid eastern slopes of the Peruvian Andes, between 1250 and 2150 m altitude (Figure 1a), and corresponds to *Yungas* montane forests. This region includes the upper watersheds of the Peruvian Amazon River and encompasses areas of little disturbed montane forests.

(b) Ombrothermic diagram of Satipo weather station for the period 1990-2009. The hydrological year in Peru is from September (year *t*) to August (year *t+1*).

(c) Validation of GPCP precipitation product (blue line) with instrumental data from the five stations shown in (a). Values have been normalized to analyze the variation of GPCP rainfall against different magnitude data. Pearson's correlation values between Nov-Oct annual precipitation from instrumental stations and GPCP data are significant (*) at $p<0.05$.

Low-elevation (<500 m) Amazonian forests lack climate seasonality (Britto, 2017), while tropical inter-Andean valleys and western slopes are typically drier. Rainfall increases with elevation up to the treeline at c. 3500 m, and relative humidity increases at these altitudes due to cooler temperatures (Catchpole, 2012). The eastern Andes/western Amazon region is the rainiest in the Amazon basin, but a complex distribution of rainfall in the eastern part of the Andes results from the steep topography and large-scale humidity transport (Killeen et al., 2007; Espinoza et al., 2015). Instrumental records are very scarce in the Amazon basin, both in distribution and in length (Marengo, 2006; Espinoza et al., 2009a). The closest weather station to our study area is in the city of Satipo (located 80 km away from the Andes range) with rainfall records from 1990 to 2009.

An extensive search through the National Service of Climatology and Hydrology of Peru (SENAMHI) confirms the lack of climatic stations near the study site. We, therefore, used a gridded product as an alternative: the Global Precipitation Climatology Project (GPCP v2.3) rain gauge and satellite-merged data, which provides continuous monthly precipitation records on a global 2.5°×2.5° grid for the period 1979 to the present (Adler et al., 2018), with proven reliability over the study region (Hurley et al., 2015). We selected the grid encompassing the 10-12.5°S and 72.5-75°W region (extracted from the KNMI Climate Explorer; https://climexp.knmi.nl/). This area contains three of the four sampling sites and the remaining one, CENE, is located <20 km away from the boundary of the GPCP grid. The selected GPCP grid was compared to Satipo weather station (656m, 1990-2009 common period), and with other available weather and hydroclimatic stations as Huayao (3350 m), Chilcayoc (3412 m), Granja Kcayra (3219 m) and Tamshiyacu (95 m) (Table S2 in Supporting Information), located farther away from the study region (Figure 1c). These stations are not as close as Satipo (the only station used as input for GPCP grid) but were used to validate the regional variability of the GPCP product.

2.2 Tree-ring analyses and precipitation reconstruction

The species sampled in this study were *Cedrela odorata*, *Cedrela nebulosa* and *Juglans neotropica*, collected in primary forests of the Central Andes of Peru (Table S1 in Supporting Information). *C. odorata* (CEOD1, CEOD2) and *J. neotropica* (JUNE) samples were collected in 2010, whilst *C. nebulosa* (CENE) collection was made during 2016. Samples were processed following standard dendrochronological methods (Stokes and Smiley, 1968), dated following the Schulman (1956) convention and measured with a precision of 0.001 mm. The visual dating was statistically checked with the program COFECHA (Holmes, 1983), and tree-ring width series were standardized with the program ARSTAN 41 (Cook & Krusic, 2005) by applying negative exponential curves or linear regression with negative or zero slopes to remove non climatic effects (Fritts, 1976). The Expressed Population Signal (EPS) and Rbar statistics are reported to evaluate the quality of the chronologies (Briffa, 1995) (Table S1 in Supporting Information).

Simple correlation analyses were computed between the four independent tree-ring chronologies (at years t, $t+1$ and $t+2$, to account for possible tree-growth delayed responses to climate) and monthly precipitation from the GPCP data set following the methods described by Fritts (1976). The period from November (year t) to October (year $t+1$) showed the highest correlations with tree-ring chronologies and was subsequently selected as a reconstruction target. Following the Schulman (1956) dating convention for the Southern Hemisphere (where the year (t) in which the ring formation begins is assigned as that ring's calendar year), each year (t) for the instrumental November-October precipitation series is composed by parts of two consecutive calendar years: year (t) = [(Nov-Dec) $_{t}$] + [(Jan-Oct) $_{t+1}$].

A stepwise multiple regression model was applied to develop the precipitation reconstruction by regressing the Nov-Oct precipitation with tree-ring chronologies. To maximize the final length of our reconstruction, we used a nested approach by which the shorter chronologies already used for reconstruction were excluded from the regression analyses to produce a longer reconstruction with the remaining series (Meko, 1997; Cook et al., 2004). A period of either 29 (1979-2007) or 32 years (1979-2010) was used to calibrate each reconstruction model using the "leave-one-out" cross-validation procedure (Michaelsen, 1987; Meko, 1997). Each model had its own calibration period. The lengths of the four independent chronologies are different, thus the resulting precipitation reconstruction (Model 1, Table 1) developed with all the chronologies was limited by the initial year of the shorter one (CENE,

1883) and the final year of CEOD2 and JUNE (in 2009). As we allowed the use of these predictors lagged at *t+1* and *t+2*, the selection of JUNE at *t+1* as a predictor limits the final year of Model 1 to 2008. We developed a second model which allowed extending the reconstruction back to 1794 using the chronology CEOD2 (Model 2, Table 1). However, we discarded the first 23 years from this second reconstruction because of the large changes in variance related to the poor sample depth in those early years. Finally, we added two more years to the reconstruction (Model 3, Table 1) in order to extend it to recent years, without losing predictive ability with the model. To generate the final nested reconstruction, we spliced together the segments from each model, adjusting their variance to that of the best replicated model (Model 1). The explained variance between observed and predicted values for each model was assessed by the coefficient of determination adjusted for loss of degrees of freedom R^2 ($R^2 adj$). We computed the reduction of error (RE) statistics (Fritts, 1976; Cook et al., 1994) to account for the relationship between the actual value and its estimate. The root mean square error of validation (RMSEv; Weisberg, 1985) and the standard error of estimate (S*e*) were calculated as an estimate of the uncertainties of the reconstructions; Durbin-Watson test (Ostrom, 1990) determines the degree of auto-correlation of the residuals. The variance inflation factor (VIF) was used to evaluate the possibility of multicollinearity in the predictors (Ostrom, 1990): a VIF close to 1 means low or no multicollinearity (Haan, 2002).

2.3 Identification of hydroclimatic variability, cycles and large-scale climate forcings

To detect precipitation trends within the tree-ring based reconstruction, we estimated the recurrence rate of drought (≤10th percentile) and pluvial (≥90th percentile) events utilizing a kernel estimation technique with a Gaussian function and 50-year bandwidth. This procedure allows the detection of nonlinear and non-monotonic trends without imposing parametric restrictions, and a smooth kernel function produces a more realistic estimation of drought and pluvial recurrences. We calculated a confidence interval at the 95% level based on 2000 bootstrap resampling steps (Cowling et al., 1996) to estimate the bias and variance properties of drought recurrence in the reconstruction. The kernel estimation, bandwidth selection, and bootstrap algorithm were computed in the free R Project platform software (R Core Team, 2016). To assess the intervals of low and high precipitation, we ranked periods of one, five and ten years according to their departure from the mean. The lengths of the windows were defined to provide a wider context for the occurrence of droughts and pluvials.

Spectral analyses were applied to identify the main oscillatory variability in the reconstruction. The Multi-Taper Method (MTM; Mann and Lees, 1996) was used to extract the cycles that explained the significant percentage of variance using Continuous Wavelet Transform analysis (WT; Grinsted et al., 2004). The WT localizes changes in the periodicities across the reconstruction. The decomposition of the reconstruction's main oscillatory modes was developed using Singular Spectral Analysis (SSA; Vautard and Ghil, 1989). To measure the common variance as a function of frequency, we conducted coherence spectral analyses (Jenkins and Watts, 1968) between the reconstructed precipitation, the mean November-October Niño 3.4 SST (1950-2010 period) and the mean November-October AMO index (1854-2010 period). The AMO index (Huang et al., 2017) was extracted from https://climexp.knmi.nl/. Additionally, we correlated our reconstruction with several ENSO indexes from different Pacific regions (see Table S3 in Supporting Information). Niño indexes were extracted from https://www.psl.noaa.gov/data/climateindices/list/.

Spatial correlation patterns between sea surface temperature (SST; GISSTv2.2 dataset, Kalnay et al., 1996) and the reconstructed precipitation were conducted to identify the large-scale modes of climate forcings over our study area. The spatial correlation between the reconstructed precipitation and the outgoing longwave radiation (OLR) was also calculated to identify the areas of deep convection over South America that influence on tropical montane Andes precipitation. Additionally, the reconstructed precipitation data were compared with the continental precipitation gridded dataset from the Climatic Research Unit (CRU TS v4.01) to assess spatial representativeness of the signal captured by the reconstruction. The NCEP-NOAA data available at the Physical Sciences Laboratory webpage were used to conduct the spatial correlation analyses (https://www.esrl.noaa.gov/psd/data/correlation/).

3 Results

3.1 Precipitation reconstruction and recurrence of dry and wet events

The GPCP gridded product presents significant correlations with stations located in or near the grid (Satipo: r=0.79, p<0.05, Huayao: r=0.54, p<0.05) (Figure 1c). The stations located above 3400 m (Chilcayoc: r=0.49, p<0.05) or farther away from the study area (Granja Kcayra: r=0.43, p<0.05) show lower (but still significant) correlations with precipitation from this GPCP grid. Interestingly, the correlation between GPCP and streamflow data from Tamshiyacu hydrometric station (r=0.57, p<0.05, period 1984-2017) at the Amazon River (located in Iquitos, at 850 km from our study site) was comparable to the correlations with stations located in the vicinity of the study area.

Tree-ring width chronologies show good replication and intercorrelation among radii (Rbar), EPS mean values above 0.85 indicate that the internal variance in each chronology corresponds to a common signal (Table S1 in Supporting Information). The comparison between the reconstruction models and GPCP precipitation suggests high skills for reconstructing precipitation for the November-October period, accounting for (R^2adj) 68% (1883-2008, Model 1), 30% (1817-2007, Model 2) and 44% (1883-2010, Model 3) of the precipitation variability during the calibration period (Table 1). The (lower) standard errors of the estimate (S*e*) are consistent with the (higher) skills in the regression models. According to the Durbin-Watson test, the residuals of the regression models are not significantly autocorrelated (DW=2). The three models successfully passed the verification process (positive RE and significant RMSEv), which implies significant predictive accuracy of tree-ring chronologies to infer past changes in precipitation. Additionally, the tree-ring chronologies' VIF, when used as predictors for the reconstructed period, had an average value of 1.23, indicating independence (low correlation) among chronologies.

The final nested reconstruction covers the period 1817 to 2010 AD and shows important interannual to multidecadal variability throughout the past 194 years for precipitation (November-October, R^2_{adj}=0.68, p<0.001) over the Amazonian Andes of Peru (Figure 2a). The reconstruction presents several multidecadal periods of precipitation below and above the average (low frequency variation in Figure 2b), but a steady drop in precipitation is observed during recent years (Figure S1 in Supporting Information), which is also reflected in the negative trend and persistent dry years in the instrumental and GPCP precipitation series (see Figure 1c). The analysis of drought and pluvial occurrences (Figure 2c) reveals that the recurrence of dry years was higher during the 1817 to 1870 period, with a return interval of about seven years for droughts below the 10th percentile. A second jump in drought (<P10) recurrence every seven to eight years is seen in recent decades, suggesting an increasing trend in drought occurrence from ~1975 to the present. On the contrary, the frequency of pluvials was high from 1880 and especially in the first decades of the twentieth century (1910-1940). However, the recurrence of high rainfall is decreasing in recent decades as the frequency of drought events tends to be higher.

The intervals of low and high precipitation were grouped into periods of 1, 5 and 10 years and ranked according to their severity from 1 to 5 (Table 2). Extreme one-year droughts appear well distributed throughout the twentieth century (1901, 1936, 1944, 1962 and 2008). Nevertheless, the years within the decade 2000 to 2009 rank first in the 1-yr (2008) and 5-yr (2004-2008) period, and second in the 10-yr (2000-2009) period, indicating that the last decade has been the driest in the 194-year precipitation reconstruction. The period 1970 to 1979 also appears in the ranking as the top third (5-yr) and fourth (10-yr) of the driest years. On the other hand, three out of the five wettest single events recorded by the reconstruction appear during the last two decades in the years 1981, 1995 and 2010. The interval between 1915 and 1933 ranks several times as the wettest 5-yr (first, third and fifth) and 10-yr (first and fifth) periods, confirming that many of the highest pluvials occurred during the first half of the twentieth century.

3.2 Interannual and multidecadal variability and large-scale climatic forcings

The spectral analysis MTM indicates that the precipitation reconstruction over the Amazonian Andes of Peru contains significant signals of variability at interannual to multidecadal scales over the past 194 years, with quasi-periodicities at 2.5, 5.1 and 41.6 years (Figure 3a). Using the singular spectral analysis SSA, we found that these quasi-cycles explain 8%, 8.4% and 13.1% of the total variance, respectively (Figures 3b-d). The wavelet analysis shows significant periodicities across the precipitation reconstruction with most significant oscillatory modes associated with interannual variability (2-7 years) during the 1940-2000 period, and a strong and significant multidecadal variability (40-60 years) between 1850 and 1975 (Figure 3e).

We explore possible relationships between our reconstruction and ENSO indices from different Pacific Ocean regions. Pearson r coefficients of -0.34 were obtained between Niño 1+2 and Niño 3 regions for the period 1950-2010 (critical r = ± 0.252; 95% confidence level). In addition, significant r Pearson coefficient of -0.31 was obtained for the same period but using the Niño 3.4 region. Given the similar correlations, we performed further analyses with Niño 3.4 index. More details about correlations between our reconstruction and several ENSO indexes are summarized in Table S3 in Supporting Information.

Coherence spectral analyses indicate that the Nov-Oct precipitation reconstruction captures interannual to multidecadal variability, with significant values (Figure 4). These bandwidths contain the largest proportion of the reconstructed variance as shown above.

The Pearson correlation field between SST and our reconstruction for the 1950-2010 period shows a clear ENSO-like pattern across the Pacific Ocean, with significant and negative correlation values between the precipitation reconstruction and sea surface temperatures in the tropical Pacific region (Figure 5a). SST correlations display the typical west-east gradient along the Equator, reaching maximum values in the vicinities of the South American coasts of

Colombia, Ecuador and northern Peru (Tedeschi et al., 2013). Above- (below) average temperatures in the tropical Pacific Ocean [coherent with El Niño (La Niña), the warm (cool) phase of ENSO] result in below- (above) average precipitations in the tropical Andes of Peru (Garreaud et al., 2009; Sulca et al., 2018). Another important factor influencing rainfall, is brought by the significant and negative correlations between our precipitation reconstruction and the tropical north Atlantic Ocean temperatures (Figure 5a), suggesting that other sources of variability such as the intertropical Atlantic SSTs may have an important influence in the rainfall of the study region. On the other hand, the main moisture source over the Yungas montane forests is the tropical lowlands east of the Andes, as revealed by the OLR correlations over the Amazon basin (Figure 5b). As OLR is used to distinguish areas of deep tropical convection (Liebmann & Smith, 1996), negative (positive) correlations indicate higher (lower) cloud cover, and thus precipitation, over the area.

We evaluate the spatial correlation between the observed (GPCP) and reconstructed tropical Andes precipitation with gridded (0.5 x 0.5°) November-October precipitation from the University of Delaware dataset (U.Del; Willmott and Matsuura, 2001) over tropical and subtropical South America (12°N-35°S; Figure 6). The two spatial correlation maps show significant positive correlations across the central tropical Andes in Peru, thus corroborating the spatially coherent signal of precipitation over the region, as obtained by comparing the GPCP precipitation with data from a network of climatic and hydrometric stations (Figure 2a-c). Furthermore, there are positive correlations across a large area in the Amazon basin as well as over Bolivia and northern Argentina (distinct in Figure 6b). The maps also show negative correlations over the coasts of Ecuador and northern Peru, the Amazon lowlands in north-eastern Peru, as well as eastern Brazil and south-eastern South America, which correspond to the SACZ see-saw activity region (Diaz & Aceituno, 2003). It is worth noting that the correlation coefficients between the U.Del gridded precipitation and the GPCP observations (Figure 6a) show comparatively lower values than those for the precipitation reconstruction (Figure 6b) due to the different temporal window used for the correlations (32 vs. 61 years, respectively). Even though Figure 6b shows larger areas of spatial correlation, both maps are capturing the general circulation pattern of the monsoon precipitation over South America.

4 Discussion

4.1 A new precipitation reconstruction for the tropical Andes

We report here the first annually-resolved precipitation reconstruction for the tropical Andes of Peru based on growth rings of *Cedrela odorata*, *Cedrela nebulosa* and *Juglans neotropica* tree species, extending the short instrumental record (1979-2010) back to 1817. Our composite reconstruction, which covers the last 194 years (1817-2010) of hydroclimatic variability, is based on 120 tree-ring width series with measures of dendrochronological quality (Table S1 in Supporting information) comparable to those reported for similar species in the subtropical Andes (Ferrero et al., 2015). The final nested precipitation reconstruction has good verification and calibration statistics. The most replicated model explains 68% of the total variance, which is higher than other precipitation reconstructions in tropical South America. Previous hydroclimatic reconstructions developed in northwestern Argentina (Ferrero et al., 2015), southern Ecuador (Pucha-Cofrep et al., 2015), southern Bolivia (López et al., 2017), eastern equatorial Brazil (Granato-Souza et al., 2018), and eastern Brazil (Pereira, 2018) typically accounted for 35 to 54% of precipitation variability during calibration periods. This new reconstruction extends the dendroclimatological studies from the subtropical Andes of Argentina into the montane tropical environments of South America.

The use of the GPCP precipitation product responds to the lack of instrumental data for the area except for a single station located in Satipo, with complete data only available starting in 1990. This data shortage constitutes one of the main limitations for the use of traditional precipitation reconstruction procedures. The use of the leave-one-out technique is especially useful for short instrumental data sets in palaeoclimatic studies (Barría et al., 2018). Despite this limitation, the GPCP gridded data are significantly correlated to meteorological stations throughout the area and the gauge station located several hundred kilometres away in the Amazon River. Thus, the hydroclimatic signal displayed by GPCP precipitation gridded product shows a spatial pattern representative of large tropical Andean basins

4.2 Frequency of drought and pluvials

The precipitation reconstruction shows decadal to multidecadal variations with several below- and above-the-mean precipitation intervals (Figure 2b). The observed dry and wet periods identified in the reconstruction are in agreement with previous studies developed for the Amazon basin. The earliest drought period registered in our reconstruction from 1817 to the 1870s, has been described by Jenkins (2009) as occurring between 1817 and 1850 based on a 189-year *Cedrela* chronology (1817-2006) located in southeastern Peru (Madre de Dios region). The rainfall reconstruction based on the Cascayunga Cave speleothems from northeast Peru (6°05’S, 77°13’W, 930 m), shows a steady decrease in rainfall values from the 1800s with a noticeable drop around the 1840s (Reuter et al., 2009). In addition, a sediment record from Lake Limón located in the western Amazon basin of Peru (6°43’S, 76°14’W, 600 m) shows that rainfall at the beginning of the 19th century was below the mean until ~1875 (with heavy droughts around 1820 and 1840) (Parsons et al., 2018). After 1875, the precipitation signal in the lake record continues to increase and authors describe a continuous wet period from 1900 to 1940-50 in their lake sediment records. This coincides with the low-frequency patterns observed in our precipitation reconstruction with the period ~1920 to 1930 and 1950 to 1960 as the wettest recorded in our tree-ring records (see Table 2).

Frequency analyses of severe events over our precipitation reconstruction (Figure 2c) reveal that high precipitation events (above the 90th percentile) occurred from the 1880s to 1970, with a peak in the occurrence of very wet events from 1930 to 1950. On the other hand, severe low precipitation events (below the 10th percentile) were recurrent from 1817 to 1870 and again from 1980 to the present. This drying trend in recent decades is recorded during the year 2000 to 2009, as the top dry period in our precipitation reconstruction (Table 2). Marengo and Espinoza (2016) suggested that there is a general decrease in the precipitation trend in the Amazon basin, probably related to the increase of interannual variability. The occurrence of precipitation events below the 10th percentile recorded in our reconstruction has increased from 7 to 8 years during the last two decades, but three events of very high precipitation have been registered in the last years (1981, 1995 and 2010; Table 1). This intensification in the interannual variability has been recorded across the Amazon, yet with different magnitudes and even opposite signs given the size of the basin and heterogeneous climate responses. For instance, Barichivich et al. (2018) found for the Amazon River that the frequency of severe floods over the 1903-2015 period has increased from one extreme flood every 20 years during the first half of the 20th century to one about every 4 years from the 2000s to the present.

4.3 Precipitation reconstruction and atmospheric circulation linkages

Most droughts recorded in our reconstruction and the region can be linked to El Niño episodes or tropical warm North Atlantic conditions (Marengo et al., 2016; Jimenez et al., 2019). For the Peruvian Amazon-Andes region, Lavado Casimiro et al. (2013) demonstrated that rainfall is less abundant during El Niño (and more abundant during La Niña). Sulca et al. (2018) showed that during El Niño events, the dominant feature is the reduction in precipitation in the tropical Andes of Bolivia, Peru and Ecuador. The dominant oscillatory modes in our tropical Andean precipitation reconstruction show major wavelengths at 2.5 and 5.1 years (16.4% of the total explained variance in precipitation) and are consistent with the classical ENSO band (2 to 8 years; Deser et al., 2010). We confirmed the high significance of this annual mode of variability with cross-spectral analysis between our tree-ring reconstruction and Niño 3.4 index (Figure 4). The amplitude of this component varies over the reconstruction with significant signal from 1940 onwards (Figure 3e). The annual spectral characteristics have been described for tree-ring hydroclimatic records in the Andes, where ENSO plays an active role in modulating local climate (e.g. northern coastal Peru, López et al., 2006; Altiplano, Morales et al., 2012; temperate-Mediterranean Chile, Christie et al., 2011) and these non-stationary periodicities have been previously reported in ENSO reconstructions (Li et al., 2013).

Pacific SST anomalies associated with ENSO play a primary role in modulating the interannual intensity of precipitation over the tropical Andes (Lavado Casimiro et al., 2013). Our precipitation reconstruction is significant and negatively correlated to SSTs, showing a clear ENSO-like pattern with higher correlation in the equatorial eastern Pacific Ocean (compatible with eastern ENSO; Figure 5a). Sulca et al. (2018) documented that reduced rainfall in the eastern Andean slopes of Peru is more associated with surface warming in the eastern equatorial Pacific and westerly wind anomalies. During summer, a high pressure system (the Bolivian High; Silva Dias et al., 1983) allows the entrance of moist air influx from the Amazon basin onto the central Andes, feeding convective storms and producing precipitation. However, this system is quite variable and tends to weaken in response to suppressed convective activity over the Pacific Ocean (i.e. related to El Niño) (Sulca et al., 2016). Sulca et al. (2018) also showed that warm ENSO phases in the eastern equatorial Pacific are negatively correlated with precipitation along the "rainfall hotspots" in the eastern Andean slopes of southern Peru (our study area), Bolivia, and adjacent Amazon plains. On the contrary, enhanced precipitation prevails along the coasts of Ecuador and northern Peru as well as in the northeastern Amazon of Peru. These results are expressed by the correlations between U.Del continental gridded precipitation, GPCP precipitation (Figure 6a) and our tree-ring precipitation reconstruction (Figure 6b) showing the same spatial patterns of precipitation related to El Niño events. The spatial correlation between OLR and the tree-ring reconstruction (Figure 5b) is higher over the monsoon core region, where deep convection is established during the mature phase of the SAMS (Vuille et al., 2012), and also over the western Amazon region where precipitation increases in the eastern slopes of the Andes (Espinoza et al., 2009a). The above is consistent with the spatial precipitation pattern over the Amazon and along the eastern Andes from Peru to northern Argentina (as in Figure 6b) coinciding with the SALLJ region. This moisture transport is linked with an opposite sign anomaly (also observed by Sulca et al., 2016) over eastern South America and the adjacent Atlantic Ocean (as reflected by the positive OLR values in Figure 5b, and consequently reduced precipitation) associated with the SACZ activity, the other major feature of the South American monsoon.

Rainfall variability in the Andean-Amazon region area, however, is not fully explained by ENSO events (Yoon & Zeng, 2010; Joetzjer et al., 2013; Jimenez et al., 2019). According to Zhou and Lau (2001) the second mode of summer rainfall variability over South America displays a significant signal over the Atlantic and varies at decadal timescale; Chiessi et al. (2009) showed with marine sediment records that Atlantic SST variations play a significant role in modulating multidecadal SAMS variability. The second oscillation which appears in our precipitation reconstruction is a long-term waveform centered at 41.6 years (Figure 3). Previous studies indicated that changes in the Atlantic SST variability reflect a low-frequency mode at 65 to 80 years, the Atlantic Multidecadal Oscillation (AMO; Enfield et al., 2001). Cross-spectral coherence computed for our tree-ring reconstruction and AMO index (Trenberth and Shea, 2006) shows that both records are in phase at a period of ~37 years (Figure 4). The ~40-yr mode in our tree-ring reconstruction is similar to the dominant mode of variability reported from a tree-ring AMO reconstruction bordering the North Atlantic (~42.7-yr; Gray et al., 2004) and the Bosumtwi lake records used to reconstruct the Western African monsoon was related to AMO variations (33 to 42-yr; Shanahan et al., 2009) (see our Figure S2 in Supporting information).

SST fluctuations in the tropical Atlantic appear to be an important forcing for rainfall fluctuation in the upper Andean basins of the Amazon in Peru. Lavado Casimiro et al. (2013) showed that when the northern tropical Atlantic is warmer than the southern, the Amazon-Andes in Peru receive less water vapor than usual, resulting in reduced rainfall. Yoon and Zeng (2010) also showed that positive (negative) temperatures over the tropical North Atlantic (EQ-20°N) are negatively (positively) correlated with interannual variability of Amazon rainfall. This oceanic region coincides with the area displaying significant (and opposite) correlations with our precipitation reconstruction for a 50-year period (Figure 5a). A warm anomaly in the north Atlantic and a weak cold anomaly in the South Atlantic draw the rainfall belt northward, leading to subsidence (low precipitation) over the southern and western Amazon basin (Cox et al., 2008; Marengo and Espinoza, 2016). Hua et al. (2019) also show for the period 1950-2017 that Amazon precipitation anomalies and negative correlation between the Atlantic north-south gradient are stronger when considering decadal to multidecadal scales (-0.87, $p<0.01$), which at the time are highly correlated with the AMO. Moreover, Jones and Carvalho (2018) demonstrate that during 1900 and 2010, the AMO phases produce periods of high/low SALLJ activity on the eastern slopes of the Andes, linked to precipitation anomalies in decadal to multidecadal scales. Many prominent features in global climate multidecadal variability have been related to AMO (Knight et al., 2006); the multidecadal signal of ~40 years found in our high-resolution tree-ring reconstruction can contribute to the interpretation and understanding of the role of the tropical Atlantic and long-term modulations on the monsoon dynamics on the Andes and tropics of South America.

Conclusions

Tropical Andean forests provide water storage and can sustain the demand for water in broader regions (Bruijnzeel et al., 2011). The capacity to dampen flows and release water during dry seasons can provide a continuous supply to downstream areas (Immerzeel et al., 2019). The upper basin of the Peruvian Amazon is highly dependent on the precipitation concentrated during the spring-summer season. Intense precipitation events can cause flooding and landslides, but drought events can result in major loss of economic (i.e. agriculture) activities (Young & León, 2009; Rodríguez-Morata et al., 2018). The precipitation dynamics in the tropical Andes are changing due to rapid global warming and increasing human pressure on the environment. These changes affect not only biodiversity and forest conservation but also increasingly affect local population's demand for water. We developed a multi-century perspective for the precipitation variability in the tropical Andes-Amazon region of South America, an area that lacks reliable instrumental data to evaluate long-term climatic variations. The new 194-year long tree ring-based precipitation reconstruction provides new information on the dynamics and behavior of the South American monsoon at high and low frequency. Dry and wet interannual and decadal periods, recorded in instrumental data and by proxy records developed for the region, were identified in our precipitation reconstruction. ENSO is a key modulator of Andes-Amazon climatic interannual variability and our reconstruction also indicates that conditions related to multidecadal changes in the Atlantic temperatures have modulated extended wet and dry periods of precipitation in the tropical Andes.

The hydroclimate information captured by our high-resolution precipitation reconstruction can identify the main large-scale climatic forcings that have influenced precipitation at interannual-to-multidecadal scales over the Andes-Amazon region during the past two centuries. Our reconstruction is capturing the main features of the monsoon system dynamics over tropical and subtropical South America. The record showed here emphasizes the need for sampling long-lived tree specimens along the tropical Andes. The annual resolution of the growth rings and the high sensitivity to climate, reflect with great detail the temporal variations and spatial patterns of instrumental series. This allows us to characterize climate on annual time scales for almost two hundred years. The expansion of dendrochronological networks in the mountain tropics and the development of additional tree-ring derived proxies (i.e. stable oxygen and carbon isotopes), can help improve our understanding on the precipitation variability and South American monsoon dynamics along the Andes and neighbouring regions. Historical land-surface changes in montane forests, recent large burning events in the Amazon and their resulting effects on the hydrological cycle in the sub/tropical Andes regions are yet to be assessed.

Acknowledgments

This research was supported by Programa Bosques Andinos (PBA; HELVETAS Swiss Intercooperation), FONDECYT-BM-INC.INV 039-2019, ANPCyT PICT-2014-2797, FONDECYT 11161061 and FONDAP 15110009. We thank the National Meteorology and Hydrology Service (SENAMHI; https://www.senamhi.gob.pe/) from Peru, Observation Service ORE - HYBAM (http://www.ore-hybam.org/) and Drs. J. Apaéstegui and R. Espinoza for providing the instrumental records. We are deeply grateful for the manuscript revision and valuable comments by the reviewers, associate editor, Drs. S. Belmecheri, B. Luckman and R. Villalba, that improved the original version.

Data Availability Statement

Climatic and tree-ring data sets analysed and/or generated in the study is available at http://www.cr2.cl/datos-dendro-amazonas-peru/ and upon request from the authors (mferrero@mendoza-conicet.gob.ar; erequena@continental.edu.pe).

References

Adler, R. F., Sapiano, M. R. P., Huffman, G. J., Wang, J-J., Gu, G., Bolvin, D., et al. (2018). The Global Precipitation Climatology Project (GPCP) monthly analysis (new version 2.3) and a review of 2017 global precipitation. *Atmosphere*, *4*(4), 138. https://doi.org/10.3390/atmos9040138

Apaéstegui, J., Cruz, F. W., Sifeddine, A., Vuille, M., Espinoza, J. C., Guyot, J.-L., et al. (2014). Hydroclimate variability of the northwestern Amazon Basin near the Andean foothills of Peru related to the South American Monsoon System during the last 1600 years. *Climate of the Past*, *10*(6), 1967-1981. https://doi.org/10.5194/cp-10-1967-2014

Apaéstegui, J., Cruz, F. W., Vuille, M., Fohlmeister, J., Espinoza, J. C., Sifeddine, A., et al. (2018). Precipitation changes over the eastern Bolivian Andes inferred from speleothem ($\delta^{18}O$) records for the last 1400 years. *Earth and Planetary Science Letters*, *494*, 124-134. https://doi.org/10.1016/j.epsl.2018.04.048

Barichivich, J., Gloor, E., Peylin, P., Brienen, R. J. W., Schöngart, J., Espinoza, J. C., & Pattnayak, K. C. (2018). Recent intensification of Amazon flooding extremes driven by strengthened Walker circulation. *Science Advances*, *4*(9), eaat8785. https://doi.org/10.1126/sciadv.aat8785

Barria, P., Peel, M. C., Walsh, K. J., & Muñoz, A. (2018). The first 300-year streamflow reconstruction of a high-elevation river in Chile using tree rings. *International Journal of Climatology, 38*(1), 436-481. https://doi.org/10.1002/joc.5786

Barthem, R., Marques, M., Charvet, P., & Montag, L. (2005). Amazon River Basin: I – characterization and environmental impacts due to deforestation. In E. Tiezzi, et al. (Eds.), *Ecosystems and Sustainable Development V* (Vol. 81, pp. 615-625). WIT Press.

Bird, B. W., Abbott, M. B., Vuille, M., Rodbell, D. T., Stansell, N. D., & Rosenmeier, M. F. (2011). A 2,300-year-long annually resolved record of the South American summer monsoon from the Peruvian Andes. *Proceedings of the National Academy of Sciences*, *108*(21), 8583–8588. https://doi.org/10.1073/pnas.1003719108

Briffa, K. R. (1995). Interpreting high-resolution proxy climate data. The example of dendroclimatology. In H. von Storch & A. Navarra (Eds.), *Analysis of climate variability, applications of statistical techniques* (pp. 77-94). Berlin, Germany: Springer Verlag.

Britto, B. (2017). Actualización de las ecorregiones terrestres de Perú propuestas en el Libro Rojo de Plantas Endémicas del Perú. *Gayana-Botánica*, *74*(1), 15-29. https://doi.org/10.4067/S0717-66432017005000318

Bruijnzeel, L. A., Mulligan, M., & Scatena, F. N. (2011). Hydrometeorology of tropical montane cloud forests: emerging patterns. *Hydrological Processes*, *25*, 465-498.

Bustamante, M. G., Cruz, F. W., Vuille, M., Apaéstegui, J., Strikis, N., Panizo, G., et al. (2016). Holocene changes in monsoon precipitation in the Andes of NE Peru based on $\delta^{18}O$ speleothem records. *Quaternary Science Reviews*, *146*, 274-287. https://doi.org/10.1016/j.quascirev.2016.05.023

Campetella, C. M., & Vera, C. S. (2002). The influence of the Andes Mountains on the South American low-level flow. *Geophysical Research Letters, 29*(17), 1826. https://doi.org/10.1029/2002GL015451

Carvalho, L. M. V., Jones, C., & Liebmann, B. (2004). The South Atlantic Convergence Zone: Intensity, form, persistence, and relationships with intraseasonal to interannual activity and extreme rainfall. *Journal of Climate, 17*, 88-108. https://doi.org/10.1175/1520-0442(2004)017%3C0088:TSACZI%3E2.0.CO;2

Catchpole, D. (2012). Orographic gradients in climate and forest cover at the Cordillera Yanachaga, Peru. PhD Thesis, University of Tasmania.

Chiessi, C., Mulitza, S., Paetzold, J., Wefer, G., & Marengo, J. (2009). Possible impact of the Atlantic Multidecadal Oscillation on the South American summer monsoon. *Geophysical Research Letters*, *36*, L21707. https://doi.org/10.1029/2009GL039914

Christie, D. A., Boninsegna, J. A., Cleaveland, M. K., Lara, A., Le Quesne, C., Morales, M. S., et al. (2011). Aridity changes in the Temperate-Mediterranean transition of the Andes since AD 1346 reconstructed from tree-rings. *Climate Dynamics*, *36*(7), 1505-1521. https://doi.org/10.1007/s00382-009-0723-4

Cook, E.R., Briffa, K.R., & Jones, P.D., 1994. Spatial regression methods in dendroclimatology: a review and comparison of two techniques. *International Journal of Climatology*, *14*, 379-402. https://doi.org/10.1002/joc.3370140404

Cook E. R., Woodhouse, C. A., Eakin, C. M., Meko, D. M., & Stahle, D. W. (2004). Long-term aridity changes in the Western United States. *Science*, *306*, 1015-1018. https://doi.org/10.1126/science.1102586

Cook, E. R., & Krusic, P. J. (2005). *Program ARSTAN, A tree-ring standardization program based on detrending and autoregressive time series modeling with interactive graphics*. Tree-Ring Laboratory, Lamont-Doherty Earth Observatory, Columbia University, Palisades, NY.

Cox, P. M., Harris, P. P., Huntingford, C., Betts, R. A., Collins, M., Jones, C. D., et al. (2008). Increasing risk of Amazonian drought due to decreasing aerosol pollution. *Nature*, *453*, 212-215. https://doi.org 10.1038/nature06960

Cowling, A., Hall, P., & Phillips, M. J. (1996). Bootstrap confidence regions for the intensity of a Poisson point process. *Journal of the American Statistical Association*, *91*(436), 1516-1524. https://doi.org/10.1080/01621459.1996.10476719

Deser, C., Alexander, M. A., Xie, S-P. & Phillips, A. S. (2010). Sea surface temperature variability: patterns and mechanisms. *Annual Review Marine Sciences*, *2*, 115-143. https://doi.org/10.1146/annurev-marine-120408-151453

Diaz, A. F., & Aceituno, P. (2003). Atmospheric circulation anomalies during episodes of enhanced and reduced convective cloudiness over Uruguay. *Journal of Climate*, *16*, 3171-3185. http://doi.or/10.1175/1520-0442(2003)016<3171:acadeo>2.0.co;2

Enfield, D. B., Mestas-Nuñez, A. M., & Trimble, P. J. (2001). The Atlantic multidecadal oscillation and its relation to rainfall and river flows in the continental U.S. *Geophysical Research Letters*, *28*(10), 2077-2080. http://dx.doi.org/10.1029/2000GL012745

Espinoza-Villar, J. C., Ronchail, J., Guyot, J. L., Cochonneau, G., Naziano, F., Lavado, W., et al. (2009a). Spatio-temporal rainfall variability in the Amazon basin countries (Brazil, Peru, Bolivia, Colombia, and Ecuador). *International Journal of Climatology*, *29*, 1574-1594. https://doi.org/ 10.1002/joc.1791

Espinoza-Villar, J. C., Guyot, J. L., Ronchail, J., Cochonneau, G., Filizola, N., Fraizy, P., et al. (2009b). Contrasting regional discharge evolutions in the Amazon basin (1974-2004). *Journal of Hydrology*, *375*, 297-311. https://doi.org/ https://doi.org/10.1016/j.jhydrol.2009.03.004

Espinoza, J. C., Chavez, S., Ronchail, J., Junquas, C., Takahashi, K., & Lavado, W. (2015). Rainfall hotspots over the southern tropical Andes: spatial distribution, rainfall intensity, and relations with large-scale atmospheric circulation. *Water Resources Research*, *51*, 3459-3475. https://doi.org/10.1002/2014WR016273

Ferrero, M. E., Villalba, R., De Membiela, M., Ferri Hidalgo, L., & Luckman, B. H. (2015). Tree-ring based reconstruction of Río Bermejo streamflow in subtropical South America. *Journal of Hydrology, 525*, 572-584. https://doi.org/10.1016/j.jhydrol.2015.04.004

Fritts, H. C. (1976). *Tree rings and climate*. San Diego, CA: Academic Press. https://doi.org/10.1016/B978-0-12-268450-0.X5001-0

Fu, R., Yin, L., Li, W., Arias, P. A., Dickinson, R. E., Huang, L., et al. (2013). Increased dry-season length over southern Amazonia in recent decades and its implication for future climate projection. *PNAS*, *110*(45), 18110-18115. https://doi.org/10.1073/pnas.1302584110

Garreaud, R., Vuille, M., Compagnucci, R., & Marengo, J. (2009). Present-day South American climate. *Palaeogeography Palaeoclimatology Palaeoecology, 281*, 180-195. https://doi.org/10.1016/j.palaeo.2007.10.032

Gloor, M., Brienen, R. J. W., Galbraith, D., Feldpausch, T. R., Schongart, J., Guyot, J. L., et al. (2013). Intensification of the Amazon hydrological cycle over the last two decades. *Geophysical Research Letters*, *40*, 1729-1733. https:// doi.org/10.1002/grl.50377

Gloor, M., Barichivich, J., Ziv, G., Brienen, R., Schöngart, J., Peylin, P., et al. (2015). Recent Amazon climate as background for possible ongoing and future changes of Amazon humid forests. *Global Biogeochemical Cycles*, *29*(9), 1384-1399. https://doi.org/10.1002/2014GB005080

Granato-Souza. D., Stahle, D. W., Barbosa, A. C., Feng, S., Torbenson, M. C. A., Assis Pereira, G., et al. (2018). Tree rings and rainfall in the equatorial Amazon. *Climate Dynamics*, *52*(3-4), 1857-1869. https://doi.org/10.1007/s00382-018-4227-y

Gray, S. T., Graumlich, L. J., Betancourt, J. L., & Pederson, G. T. (2004). A tree-ring based reconstruction of the Atlantic Multidecadal Oscillation since 1567 A.D. *Geophysical Research Letters*, *31*, L12205. https://doi.org/10.1029/2004GL019932

Grinsted, A., Moore, J. C., & Jevrejeva, S. (2004). Application of the cross wavelet transform and wavelet coherence to geophysical time series. *Nonlinear Processes in Geophysics* 11, 561-566. https://doi.org/ 10.5194/npg-11-561-2004

Haan, C. (2002). *Statistical methods in hydrology*. Iowa State Press, Iowa.

Holmes, R. L. (1983). Computer-assisted quality control in tree-ring dating and measurement. *Tree-ring Bulletin, 43*(1), 69-78.

Hua, W., Dai, A., Zhou, L., Qin, M., & Chen, H. (2019). An externally forced decadal rainfall seesaw pattern over the Sahel and Southeast Amazon. *Geophysical Research Letters*, *46*(2), 923-932. https://doi.org/10.1029/2018GL081406

Huang, B., Thorne, P. W., Banzon, V. F., Boyer, T., Chepurin, G., Lawrimore, J. H., et al. (2017). Extended reconstructed sea surface temperature, version 5 (ERSSTv5): Upgrades, validation, and intercomparisons. *Journal of Climate, 30*, 8179-8205. https://doi.org/10.1175/JCLI-D-16-0836.1

Hurley, J. V., Vuille, M., Hardy, D. R., Burns, S. J., & Thompson, L. G. (2015). Cold air incursions, δ18O variability, and monsoon dynamics associated with snow days at Quelccaya Ice Cap, Peru. *Journal of Geophysical Research: Atmospheres, 120*(15), 7467-7487. https://doi.org/10.1002/2015JD023323

Immerzeel, W. W., Lutz, A. F., Andrade, M., Bahl, A., Blemans, H., Bolch, T., et al. (2019). Importance and vulnerability of the world's water towers. *Nature*, *577*(7790), 364-373. https://doi.org/10.1038/s41586-019-1822-y

Jenkins, H. S. (2009). Amazon climate reconstruction using growth rates and stable isotopes of tree ring cellulose from Madre de Dios Basin, Peru, (Doctoral dissertation). Retrieved from Duke University Library (https://dukespace.lib.duke.edu/dspace/bitstream/handle/10161/1352/D_Jenkins_Hillary_a_200908.pdf?sequ). Department of Earth & Ocean Sciences, Duke University.

Jenkins, G. M., & Watts, D. G. (1968). *Spectral analyses and its applications*. Holden-Day, San Francisco.

Jimenez, J. C., Marengo, J. A., Alves, L. M., Sulca, J. C., Takahashi, K., Ferrett, S., & Collins, M. (2019). The role of ENSO flavors and TNA on recent droughts over Amazon forests and the Northeast Brazil region. *International Journal of Climatology*. https://doi.org/10.1002/joc.6453

Joetzjer, E., Douville, H., Delire, C., Ciais, P., Decharme, B., & Tyteca, S. (2013). Hydrologic benchmarking of meteorological drought indices at interannual to climate change timescales: a case study over the Amazon and Mississippi river basins. *Hydrology and Earth System Sciences*, *17*, 4885-4895. https://doi.org/10.5194/hess-17-4885-2013

Jones, C., & Carvalho, L. M. V. (2018). The influence of the Atlantic multidecadal oscillation on the eastern Andes low-level jet and precipitation in South America. *npj Climate and Atmospheric Science 1*, 40. https://doi.org/10.1038/s41612-018-0050-8

Kalnay, E., Kanamitsu, M., Kistler, R., Collins, W., Deaven, D., Gandin, L., et al. (1996). The NCEP/NCAR 40-Year Reanalysis Project. *Bulletin of the American Meteorological Society, 77*, 437-470

Killeen, T. J., Douglas, M., Consiglio, T., Jørgensen, P. M., & Mejia, J. (2007). Dry spots and wet spots in the Andean hotspot. *Journal of Biogeography*, *34*(8), 1357-1373. https://doi.org/10.1111/j.1365-2699.2006.01682.x

Knight, J. R., Folland, C. K., & Scaife, A. A. (2006). Climate impacts of the Atlantic Multidecadal Oscillation. *Geophysical Research Letters*, *33*, L17706. https://doi.org/10.1029/2006GL026242.

Layme-Huaman, E.T., Ferrero, M. E., Palacios-Lazaro, K. S., & Requena-Rojas, E. J. (2018). *Cedrela nebulosa*: A novel species for dendroclimatological studies in the montane tropics of South America. *Dendrochronologia*, *50*, 105-112. https://doi.org/10.1016/j.dendro.2018.06.004

Lavado Casimiro, W. S., Labat, D., Ronchail, J., Espinoza, J. C., & Guyot, J. L. (2013). Trends in rainfall and temperature in the Peruvian Amazon-Andes basin over the last 40 years (1965-2007). *Hydrological Processes*, *27*(20), 2944–2957. https://doi.org/10.1002/hyp.9418

Li, J., Xie, S.-P., Cook, E. R., Morales, M. S., Christie, D. A., Johnson, N. C., et al. (2013). El Niño modulations over the past seven centuries. *Nature Climate Change*, *3*, 822-826.

Liebmann, B., & Smith, C. A. (1996). Description of a complete (Interpolated) Outgoing Longwave Radiation dataset. *Bulletin of the American Meteorological Society*, *77*, 1275-1277.

López, B. C., Rodríguez, R., Gracia, C. A., & Sabaté, S. (2006). Climatic signals in growth and its relation to ENSO events of two *Prosopis* species following a latitudinal gradient in South

America. *Global Change Biology*, *12*, 897-906. https://doi.org/ 10.1111/j.1365-2486.2006.01138.x

López, L., Stahle, D., Villalba, R., Torbenson, M., Feng, S., & Cook, E. (2017). Tree ring reconstructed rainfall over the southern Amazon Basin. *Geophysical Research Letters*, *44*, 1-9. https://doi.org/10.1002/2017GL073363

Mann, M.E., & Lees, J. (1996). Robust estimation of background noise and signal detection in climatic time series. *Climate Change*, *33*(3), 409-445. http://dx.doi.org/10.1007/BF00142586

Marengo, J. A. (2004). Interdecadal variability and trends of rainfall across the Amazon basin. *Theoretical and Applied Climatology*, *78*(1-3), 79-96. https://doi.org/10.1007/s00704-004-0045-8

Marengo, J. A. (2006). On the hydrological cycle of the Amazon Basin: A historical review and current state-of-the-art. *Revista Brasileira de Meteorologia*, *21*(3), 1-19.

Marengo, J. A., Douglas, M. W., & Dias, P. L. S. (2002). The South American low-level jet east of the Andes during thr 1999 LBA-TRMM and LBA-WET AMC campaign. *Journal of Geophysical Research: Atmospheres*, *107*(D20), 8079. https://doi.org/10.1029/2001JD001188

Marengo, J. A., Nobre, C. A., Tomasella, J., Oyama, M. D., Oliveira, G. S., de Oliveira, R., et al. (2008). The drought of Amazonia in 2005. *Journal of Climate*, *21*, 495-516, https://doi.org/10.1175/2007JCLI1600.1

Marengo, J. A., Tomasella, J., Alves, L. M., Soares, W. R., & Rodriguez, D. A. (2011). The drought of 2010 in the context of historical droughts in the Amazon region. *Geophysical Research Letters*, *38*, L12703. https://doi.org/10.1029/2011GL047436

Marengo, J. A., & Espinoza, J. C. (2016). Extreme seasonal droughts and floods in Amazonia: causes, trends and impacts. *International Journal of Climatology*, *36*, 1033-1050. https://doi.org/10.1002/joc.4420

Marengo, J. A., Williams, E. R., Alves, L. M., Soares, W. R., & Rodriguez, D. A. (2016). Extreme seasonal climate variations in the Amazon Basin: droughts and floods. In: Nagy, L., Forsberg B., Artaxo P. (Eds.), *Interactions between biosphere, atmosphere and human land use in the Amazon Basin. Ecological Studies (Analysis and Synthesis)*, (Vol. 227, pp. 55-76). Berlin, Heidelberg, Springer.

Meko, D. (1997). Dendroclimatic reconstruction with time varying predictor subsets of tree indices. *Journal of Climate*, *10*, 687–696. https://doi.org/10.1175/1520-0442(1997)010%3C0687:DRWTVP%3E2.0.CO;2

Michaelsen, J. (1987). Cross-validation in statistical climate forecast models. *Journal of Climate and Applied Meteorology*, *26*, 1589-1600.

Morales, M. S., Christie, D. A., Villalba, R., Argollo, J., Pacajes, J., Silva, J. S., et al. (2012). Precipitation changes in the South American Altiplano since 1300AD reconstructed by tree-rings. *Climates of the Past*, *8*, 653-666. https://doi.org/10.5194/cp-8-653-2012

Novello, V. F., Cruz, F. W., Karmann, I., Burns, S. J., Strikis, N. M., Vuille, M., et al. (2012). Multidecadal climate variability in Brazil's Nordeste during the last 3000 years based on speleothem isotope record. *Geophysical Research Letters*, *39*, L23706. https://doi.org/10.1029/2012GL053936

Novello, V. F., Vuille, M., Cruz, F. W., Stríkis, N. M., Saito de Paula, M., Edwards, R. L., et al. (2016). Centennial-scale solar forcing of the South American Monsoon System recorded in stalagmites. *Scientific Reports*, *6*(1), 24762. https://doi.org/10.1038/srep24762

Novello, V. F., Cruz, F. W., Moquet, J. S., Vuille, M., de Paula, M. S., Nunes, D., et al. (2018). Two millenia of South Atlantic Convergence Zone variability reconstructed from isotopic proxies. *Geophysical Research Letters*, *45*(10), 5045-5051. https://doi.org/10.1029/2017GL076838

Ostrom, C. W. (1990). *Time series analysis: regression techniques*. Thousand Oaks, CA, SAGE Publications.

Parsons, L. A., LeRoy, S., Overpeck, J. T., Bush, M., Cárdenes-Sandí, G. M., & Saleska, S. (2018). The threat of multi-year drought in Western Amazonia. *Water Resources Research, 54*(9), 5890-5904. https://doi.org/10.1029/ 2017WR021788

Pereira, G. de A. (2018). Dendroclimatology in seasonally dry tropical forests in the São Francisco Basin, Brazil, (Doctoral dissertation). Retrieved from Repositório UFLA (http://repositorio.ufla.br/handle/1/3276Z). Universidade Federal de Lavras, Brazil.

Pereyra-Espinoza, M. J., Inga-Guillen, G. J., Morales, M. S., & Rodríguez-Arisméndiz, R. (2014). Potencialidad de *Cedrela odorata* (Meliaceae) para estudios dendrocronológicos en la selva central del Perú. *Revista de Biología Tropical*, *62*(2).

Pucha-Cofrep, D., Peters, T., & Bräuning, A. (2015). Wet season precipitation during the past century reconstructed from tree-rings of a tropical dry forest in Southern Ecuador. *Global and Planetary Change 133*, 65-78. https://doi.org/ 10.1016/j.gloplacha.2015.08.003

R Core Team (2016) *R: A Language and Environment for Statistical Computing. R Foundation for Statistical Computing*. Vienna, Austria.

Reuter, J., Stott, L., Khider, D., Sinha, A., Cheng, H., & Edwards, R.L. (2009). A new perspective on the hydroclimate variability in northern South America during the Little Ice Age. *Geophysical Research Letters*, 36, L21706. https://doi.org/10.1029/2009GL041051

Rodríguez-Morata, C., Ballesteros-Canovas, J.A., Rohrer, M., Espinoza, J.C., Beniston, M., & Stoffel, M. (2018). Linking atmospheric circulation patterns with hydro-geomorphic disasters in Peru. *International Journal of Climatology, 38*(8), 3388-3404. https://doi.org/10.1002/joc.5507

Schöngart, J., Piedade, M. T. F., Ludwigshausen, S., Horna, V., & Worbes, M. (2002). Phenology and stem-growth periodicity of tree species in Amazonian floodplain forests. *Journal of Tropical Ecology*, *18*(4), 581-597. https://doi.org/10.1017/S0266467402002389

Schulman, E. (1956). *Dendroclimatic changes in semiarid America*. Tucson, AZ: University of Arizona Press.

Segura, H., Junquas, C., Espinoza, J. C., Vuille, M., Jauregui, Y. R., Rabatel, A., et al. (2019). New insights into the rainfall variability in the tropical Andes on seasonal and interannual time scales. *Climate Dynamics*, *53*, 405-426. https://doi.org/10.1007/s00382-018-4590-8

Shanahan, T. M., Overpeck, J. T., Anchukaitis, K. J., Beck, J. W., Cole, J. E., Dettman, D. L., et al. (2009). Atlantic forcing of persistent drought in West Africa. *Science*, *324*, 377-380. https://doi.org/10.1126/science.1166352

Silva Dias, P. L., Schubert, W. H., & DeMaria, M. (1983). Large-scale response of the tropical atmosphere to transient convection. *Journal of the Atmospheric Sciences, 40,* 2689-2707. https://doi.org/10.1175/1520-0469(1983)040%3C2689:LSROTT%3E2.0.CO;2

Stokes, M., & Smiley, T. (1968). *An introduction to tree-ring dating*. Tucson, AZ: University of Arizona Press.

Sulca, J., Vuille, M., Silva, Y., & Takahashi, K. (2016). Teleconnections between the Peruvian Central Andes and Northeast Brazil during extreme rainfall events in austral summer. *Journal of Hydrometeorology*, *17*, 499-515. https://doi.org/10.1175/JHM-D-15-0034.1

Sulca, J., Takahashi, K., Espinoza, J.C., Vuille, M., & Lavado-Casimiro, W. (2018). Impacts of different ENSO flavors and tropical Pacific convection variability (ITCZ, SPCZ) on austral summer rainfall in South America, with a focus on Peru. *International Journal of Climatology, 38*, 420-435. https://doi.org/10.1002/joc.5185

Tedeschi, R. G., Cavalcanti, I. F. A., & Grimm, A. M. (2013). Influences of two types of ENSO on South American precipitation. *International Journal of Climatology, 33*, 1382-1400. https://doi.org/10.1002/joc.3519

Trenberth, K. E., & Shea, D. J. (2006). Atlantic hurricanes and natural variability in 2005. *Geophysical Research Letters*, *33,* L12704. https://doi.org/10.1029/2006GL026894

Urrutia, R., & Vuille, M. (2009). Climate change projections for the tropical Andes using a regional climate model: Temperature and precipitation simulations for the end of the 21st century. *Journal of Geophysical Research*, *114*, D02108. https://doi.org/10.1029/2008JD011021

Vautard, R., & Ghil, M. (1989). Singular spectrum analysis in nonlinear dynamics, with applications to paleoclimate time series. *Journal of Physics D*, 35, 395-424.

Vera, C., Higgins, W., Amador, J., Ambrizzi, T., Garreaud, R., Gochis, D., et al (2006). Toward a unified view of the American Monsoon systems. *Journal of Climate*, *19*(20), 4977-5000. https://doi.org/10.1175/JCLI3896.1

Vuille, M., & F. Keimig (2004). Interannual variability of summertime convective cloudiness and precipitation in the central Andes derived from ISCCP-B3 data. *Journal of Climate*, *17*, 3334-3348. https://doi.org/10.1175/1520-0442(2004)017%3C3334:IVOSCC%3E2.0.CO;2

Vuille, M., Burns, S. J., Taylor, B. L., Cruz, F. W., Bird, B. W., Abbott, M. B., et al. (2012). A review of the South American monsoon history as recorded in stable isotopic proxies over the past two millennia. *Climate of the Past*, *8*(4), 1309-1321. https://doi.org/10.5194/cp-8-1309-2012

Wang, X., Edwards, R. L., Auler, A. S., Cheng, H., Kong, X., Wang, Y., et al. (2017). Hydroclimate changes across the Amazon lowlands over the past 45,000 years. *Nature, 54*(7636), 204-207. https://doi.org/10.1038/nature20787

Weisberg, S. (1985). *Applied Linear Regression*. New York, John Wiley.

Willmott, C.J., & Matsuura, K. (2001). *Terrestrial air temperature and precipitation: monthly and annual time series (1950-1999).* Retrieved from http://climate.geog.udel.edu/~climate/html_pages/README.ghcn_ts2.html

Wortham, B. E., Wong, C. I., Silva, L. C. R., McGee, D., Montañez, I. P., Rasbury, E. T., et al. (2017). Assessing response of local moisture conditions in central Brazil to variability in regional monsoon intensity using speleothem $^{87}Sr/^{86}Sr$ values. *Earth and Planetary Science Letters, 463*, 310-322. https://doi.org/10.1016/j.epsl.2017.01.034

Yoon, J.-H., & Zeng, N. (2010). An Atlantic influence on Amazon rainfall. *Climate Dynamics*, *34*, 249-264. https://doi.org/10.1007/s00382-009-0551-6

Young, K.R. & León, B. (2009). Natural Hazards in Peru. Causation and Vulnerability. *Developments in Earth Surface Processes*, *13*(C), 165-180. https://doi.org/10.1016/S0928-2025(08)10009-8

Zhou, J., & Lau, K. M. (1998). Does a monsoon climate exist over South America?. *Journal of Climate*, *11*, 1020-1040. https://doi.org/10.1175/1520-0442(1998)011%3C1020:DAMCEO%3E2.0.CO;2

Zhou, J., & Lau, K. M. (2001). Principal modes of interannual and decadal variability of summer rainfall over South America. *International Journal of Climatology*, *21*, 1623-1644. https://doi.org/ 10.1002/joc.70

References from the Supporting Information

Ashok, K., Behera, S. K., Rao, S. A., Weng, H., & Yamagata, T. (2007). El Niño Modoki and its possible teleconnection. *Journal of Geophysical Research: Oceans*, *112*(C11). https://doi.org/10.1029/2006JC003798

Inga, J. G., & del Valle, J. I. (2017). Log-relative growth: A new dendrochronological approach to study diameter growth in *Cedrela odorata* and *Juglans neotropica*, Central Forest, Peru. *Dendrochronologia*, *44*, 117-129. https://doi.org/10.1016/j.dendro.2017.03.009

Koecke, A. V., Muellner-Riehl, A. N., Pennington, T. D., Schorr, G., & Schnitzler, J. (2013). Niche evolution through time and across continents: The story of Neotropical Cedrela (Meliaceae). *American Journal of Botany*, *100*(9), 1800-1810. https://doi.org/ 10.3732/ajb.1300059

Pennington, T. D., & Muellner, A. N. (2010). *A monograph of Cedrela (Meliaceae)*. Missouri Botanical Garden Press, dh books.

Rodionov, S. N. (2004). A sequential algorithm for testing climate regime shifts. *Geophysical Research Letters*, *31*, L09204. https://doi.org/10.1029/2004GL019448

Toro Vanegas, E., & Roldán Rojas, I. C. (2018). Estado del arte, propagación y conservación de *Juglans neotropica* Diels., en zonas andinas. *Madera y Bosques*, *24*(1), e2411560. http://dx.doi.org/10.21829/myb.2018.2411560

Yu, J. Y., Zou, Y., Kim, S. T., & Lee, T. (2012). The changing impact of El Niño on US winter temperatures. *Geophysical Research Letters*, *39*(15). https://doi.org/10.1029/2012GL052483

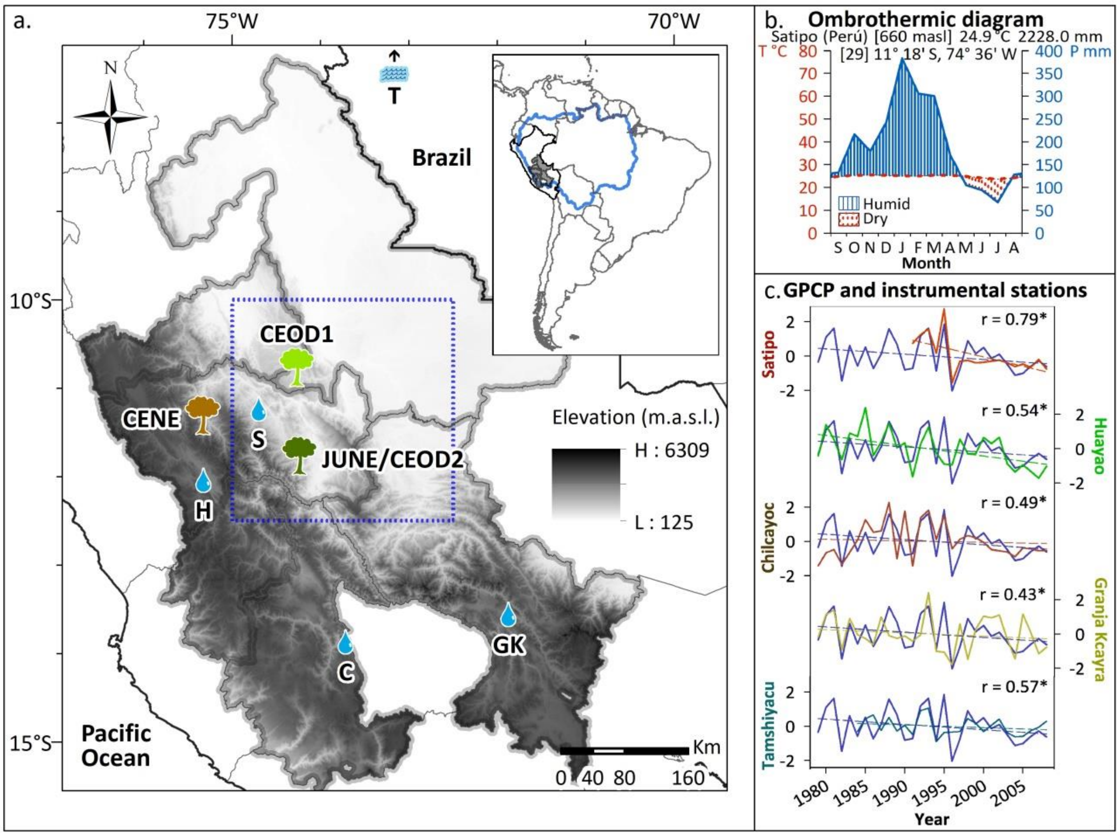

Figure 1. Map of the study sites and meteorological/hydrometric stations in the tropical Andes of Peru. (a) Location of the tree-ring chronologies (tree icons), weather stations (water drops), hydrometric station (wavy lines) and GPCP precipitation grid (blue dashed square) used for analyses. CEOD1, CEOD2, CENE and JUNE correspond to the tree-ring chronologies (Table S1 in Supporting Information). Precipitation stations are Satipo (S), Huayao (H), Chilcayoc (C) and Granja Kcayra (GK); hydrometric station is Tamshiyacu (T). The grey shaded areas are the different provinces in which tree-ring chronologies and stations are located: Ucayali (CEOD1), Junín (CENE, JUNE and CEOD2; S, H and P), Ayacucho (C) and Cusco (GK). The blue polygon in the South American map marks the Amazon basin.

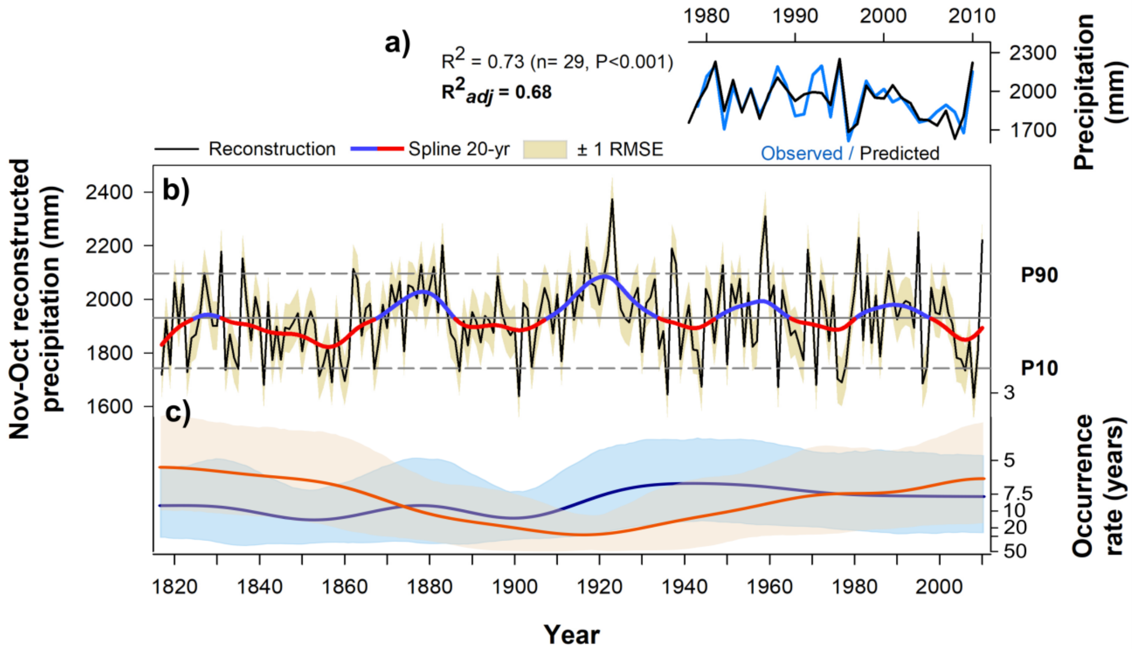

Figure 2. Tree-ring based reconstruction. (a) Comparison between GPCP (blue) and tree-ring reconstructed (black) rainfall for the 1979-2010 period. The coefficient of determination (R^2) and adjusted by degrees of freedom (R^2_{adj}) show significant positive correlations between the GPCP precipitation and tree-ring precipitation reconstruction. (b) Reconstruction of the yearly (November-October) precipitation variations in the Amazonian Andes of Peru. This nested tree-ring based reconstruction covers the 1817-2010 period. Mean (1930.9 mm, solid grey line), 90th (2096.8 mm) and 10th (1742.5 mm) percentiles (P90 and P10, dashed lines) are shown for reference in the reconstruction. The shaded area stands for the ± one root-mean-square error (RMSE), which estimates the uncertainty of the reconstructed series. A 20-year smoothing spline was used to emphasize the low frequency above (blue) and below (red) the mean. (c) Occurrence rate (in years) of severe dry (red) and wet (blue) events for the precipitation reconstruction over the Amazonian Andes of Peru for the last two centuries, calculated for the 10th and 90th percentile thresholds respectively. Shaded areas represent 95% confidence intervals.

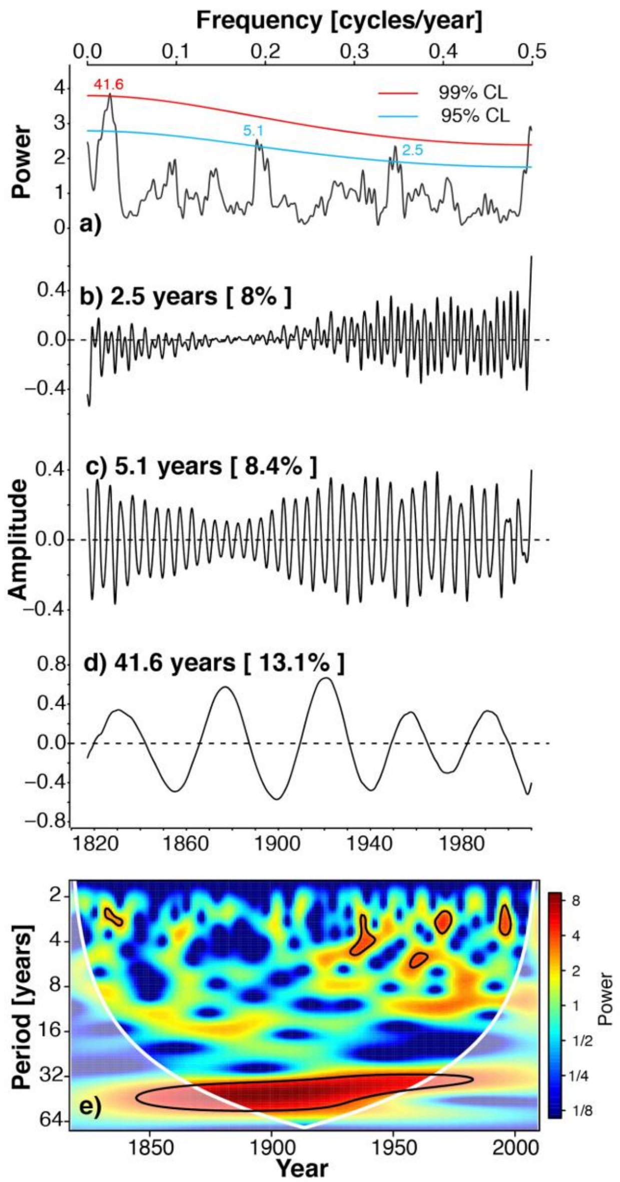

Figure 3. Oscillatory modes of variability in the precipitation reconstruction. (a) Spectral analysis of the reconstruction. Significant main modes are labeled above the 99% and 95% confidence band. (b-d) Significant oscillatory modes of precipitation variability estimated by Singular Spectral Analysis (SSA). (e) The continuous wavelet transform of our precipitation reconstruction using a Morlet adjustment. Thick black contours indicate spectral signals at 95% significance level using the red noise model. Areas outside the cone of influence are shown in a lighter shade.

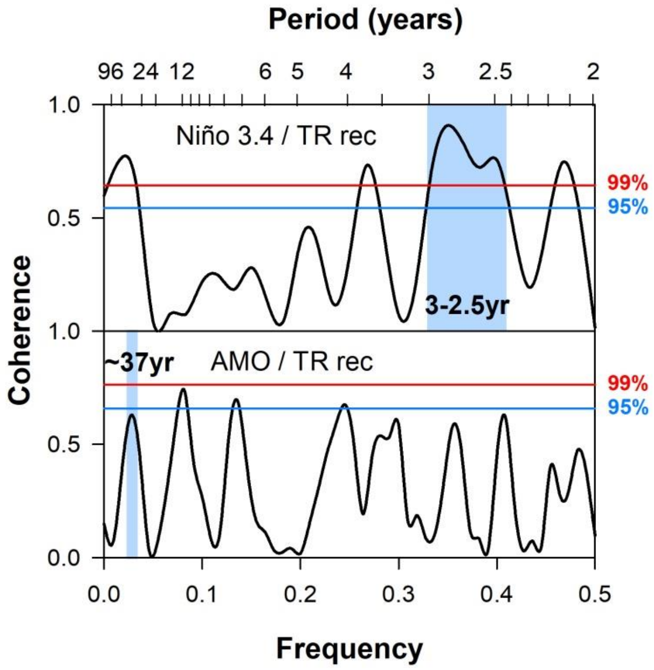

Figure 4. Cross-spectral coherence computed between the precipitation tree-ring reconstruction (TR rec) and Niño 3.4 SST (above) and AMO index (below). Horizontal lines indicate the 99 and 95% confidence intervals. Precipitation reconstruction and Niño 3.4 SST are in phase and highly coherent at a period between 2.5 to 3 years (above 99% also indicated by shading), while the precipitation reconstruction and AMO index are in phase at a period of ~ 37 years (approaching 95%, indicated by shading).

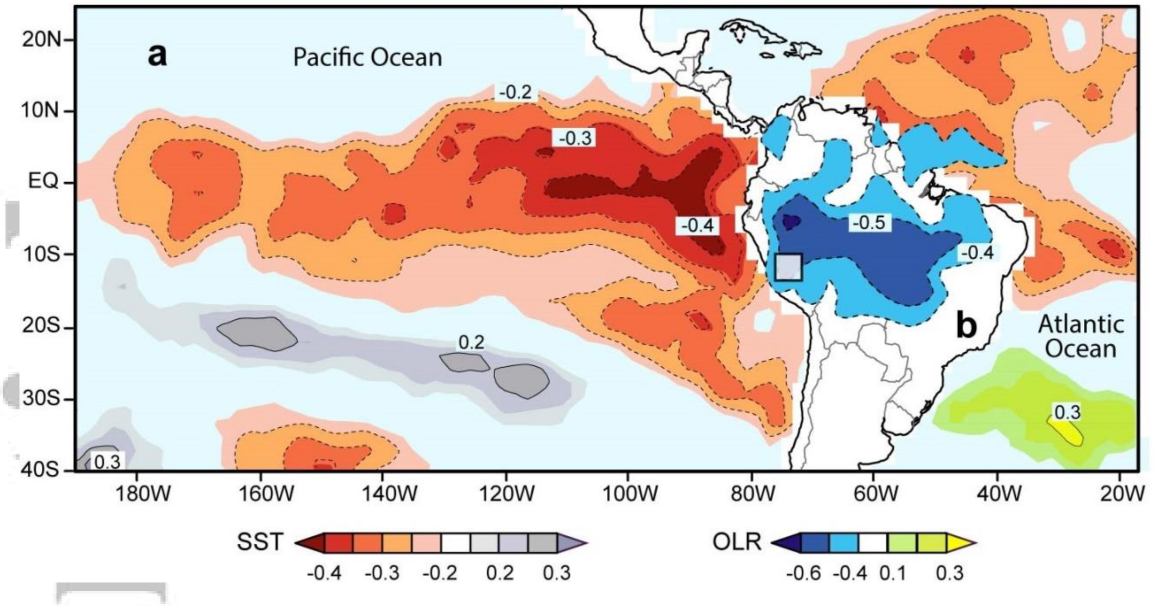

Figure 5. Spatial correlation field between annual (November-October) tree-ring precipitation reconstruction with (a) 2.5 x 2.5° gridded averaged November-October sea surface temperature (SST) over the equatorial Pacific and tropical Atlantic Oceans for the 1950-2010 period and (b) outgoing longwave radiation (OLR) over South America during the 1979-2010 period. Significant correlations ($p<0.05$) are outlined for negative (dashed lines) and positive (solid lines) values. The reconstructed precipitation region is indicated by the square over Peru.

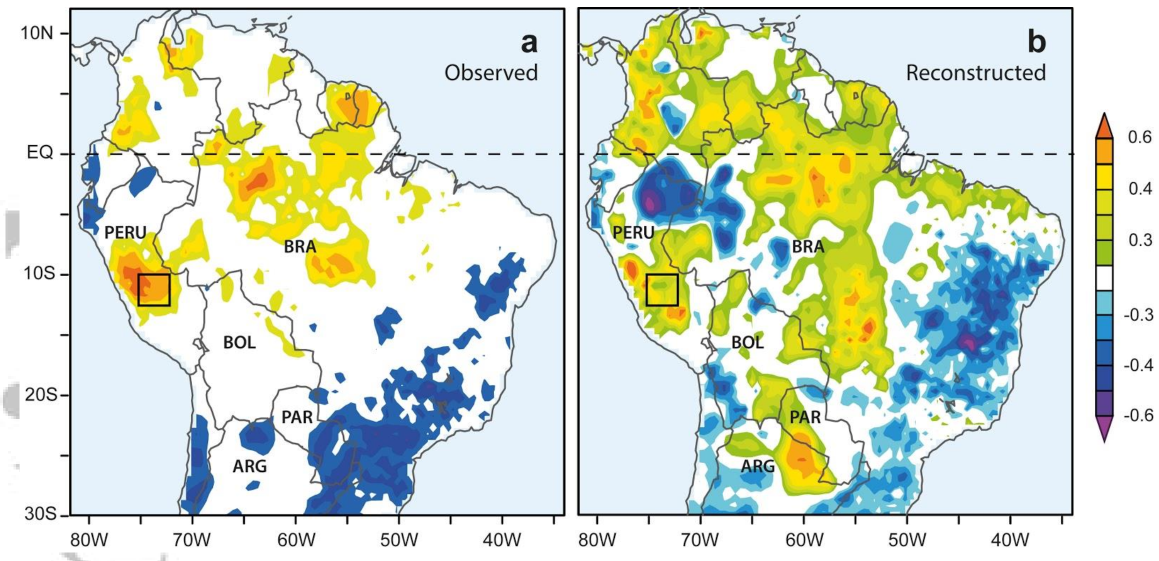

Figure 6. Spatial correlation field between the annual (November-October) 0.5 x 0.5° gridded precipitation data (University of Delaware, U.Del) over South America and (a) GPCP Nov-Oct series used for the reconstruction (1979-2010 correlation period), (b) the Nov-Oct tree-ring reconstructed precipitation (1950-2010 correlation period). Only significant correlations ($p<0.05$) are shown. The reconstructed precipitation region is indicated by the square over Peru. Countries acronyms are BRA= Brazil, BOL= Bolivia, PAR= Paraguay and ARG= Argentina.

Table 1. Calibration and verification statistics for the three independent models that constitute the final nested reconstruction, where R^2 stands for the square of the multiple correlation coefficients and R^2_{adj} is adjusted to the loss of degrees of freedom; S*e*, standard error of estimate; DW for the Durbin-Watson statistics; RE for the reduction of error and RMSEv for the root mean squared error of validation.

Model	**Predictors** (Chronologies)	**Calibration period**	**R^2/ R^2_{adj}**	**S*e***	**DW**	**RE**	**RMSEv**	**Reconstructed period**
1)	CEOD1, CEOD2, CENE, JUNE	1979-2007	0.73 / 0.68	93.15	1.92	0.60	100.51	1883-2008
2)	CEOD2	1979-2007	0.38 / 0.30	134.79	2.28	0.26	136.64	1817-2007
3)	CEOD1, CENE	1979-2010	0.53 / 0.44	124.14	2.20	0.22	144.67	1883-2010

Table 2. Rank of driest and wettest years (and their associated mean precipitation in mm/year) calculated in one, five and ten-year periods, within the 194-year tree-ring precipitation reconstruction. The precipitation for the five- and ten-year periods was obtained using a moving average, selecting the highest and lowest events with no overlapping years (1-year overlap was allowed in the ten year period).

	Droughts					
Rank	**1 year**		**5 years**		**10 years**	
1	2008	(1632.89)	2004-2008	(1754.68)	1852-1861	(1802.02)
2	1901	(1638.63)	1857-1861	(1772.38)	2000-2009	(1842.99)
3	1936	(1645.09)	1974-1978	(1801.59)	1841-1850	(1857.05)
4	1962	(1672.22)	1841-1845	(1823.33)	1970-1979	(1865.38)
5	1944	(1673.40)	1852-1856	(1831.66)	1832-1841	(1873.14)
	Pluvial					
Rank	**1 year**		**5 years**		**10 years**	
1	1923	(2379.03)	1920-1924	(2139.36)	1915-1924	(2101.77)
2	1959	(2309.84)	1957-1961	(2072.13)	1875-1884	(2049.02)
3	1995	(2250.12)	1915-1919	(2064.17)	1951-1960	(2009.70)
4	1981	(2229.33)	1879-1883	(2058.76)	1980-1989	(1993.11)
5	2010	(2220.36)	1979-1983	(2022.06)	1924-1933	(1981.47)